A Numerical Model of Precipitation from Seeded and Unseeded Cold Orographic Clouds

M. N. PLOOSTER AND N. FUKUTA

Denver Research Institute, University of Denver, Colo. 80210

(Manuscript received 28 August 1974, in revised form 8 April 1975)

ABSTRACT

This paper describes a numerical model of ice-phase precipitation from orographic clouds which includes the effects of seeding with artificial ice nuclei. The model describes the events which take place when a layer of moist air of near-neutral stability, overlain by a more stable dry layer, flows over a mountain ridge. A two-dimensional, steady-state model of the flow in the vertical plane normal to the ridge furnishes a field of the flow streamlines along which microphysical processes are followed. The cloud physics model describes the formation of the supercooled cloud, the formation of ice particles from both natural and artificial ice nuclei, and the growth and precipitation of ice particles. Growth by both vapor deposition and riming are included. Artificial ice nuclei are released from a localized source at ground level. A simple Fickian diffusion process is used to describe the vertical transport of nuclei to the cold upper region of the cloud.

The model calculates the rate of precipitation at ground level as a function of horizontal position. The dependence of precipitation efficiency on cloud top temperature is in good agreement with field observations from the Climax experiment. Substantial precipitation increases are produced by seeding clouds whose natural precipitation efficiencies are low. However, it is shown that the seeding rate required to produce a given increase in precipitation rate is a strong function of cloud temperature. The model also shows that precipitation rates depend upon the activity of the ice nuclei as a function of temperature.

1. Introduction

This paper describes the development of a numerical model of orographic ice-phase precipitation which includes the effects of seeding with artificial ice nuclei. The model was designed to fulfill three objectives: 1) to estimate the efficiency of natural precipitation from cold orographic clouds; 2) to simulate the changes in precipitation resulting from seeding with artificial ice nuclei from sources at ground level, and thus to define the opportunity for seeding; and 3) to investigate the changes in precipitation produced by variation of seeding techniques (amount of nucleant released, type of nucleant, and location of source). In this last respect, the goals were to use the model to optimize precipitation augmentation by varying seeding techniques, and to compare the relative effects of AgI and the organic ice nucleants developed in the Cloud Physics Laboratory of the Denver Research Institute.

These design objectives determined the structure of the model. Comparison of seeded and unseeded precipitation requires explicit consideration of the number, activity and distribution of both natural and artificial ice nuclei, and of the growth of ice crystals formed therefrom. Thus the core of the model is the sub-model of cloud microphysics, which describes the partitioning of water substance between vapor, liquid and solid phases. A simple, two-dimensional, steady-state flow sub-model provides a field of flow streamlines along which microphysical processes are followed in space and time. The simulation of seeding with ice nuclei from ground-level sources necessitates a third sub-model to describe the transport and vertical diffusion of ice nuclei.

The model was designed to be applied to winter orographic systems typical of the Colorado Rocky Mountain area. These systems are often characterized by passage of a lower moist layer of near-neutral stability, capped by a more stable dry upper layer. Thus the model considers a two-layer atmosphere with microphysics in the lower layer only.

2. The flow model

We employ a relatively simple, two-dimensional, steady-state model of the flow in a two-layer atmosphere. Since the treatment largely follows conventional lines and is described in more detail elsewhere (Fukuta *et al.*, 1973), only a brief description is given here. Flow takes place in the vertical (x,z) plane normal to a long mountain ridge. Given a vertical sounding of the "undisturbed" atmosphere well upwind of the mountain ridge, and expressing the variations in thermodynamic and flow variables as small perturbations from this initial state, the equations for conservation of mass, momentum and energy can be reduced to a linear elliptic partial differential equation in one unknown,

e.g., the vertical velocity w. Employing the Fourier transformation in the x coordinate, one obtains

$$\frac{d^2\hat{w}}{dz^2}+(l^2-k^2)\hat{w}=0, \tag{1}$$

where

$$\left[\frac{\rho_0(0)}{\rho_0(z)}\right]^{\frac{1}{2}}w(x,z)=\int_{-\infty}^{\infty}\hat{w}(k,z)e^{ikx}dk, \tag{2}$$

$$l^2\approx\frac{g}{U_0{}^2}\frac{d\ln\theta_0}{dz}, \tag{3}$$

where:

$\rho_0(z)$ air density in the initial state
$\theta_0(z)$ potential temperature in the initial state
$U_0(z)$ horizontal velocity in the initial state
g gravitational acceleration
k horizontal wavenumber
l^2 the "Scorer parameter."

We assume that l_1^2 and l_2^2, the values of the Scorer parameter in the lower and upper layers respectively, are constant, with $l_2^2\geqslant l_1^2\geqslant 0$. When l^2 is constant, the general solution of (1) is

$$\hat{w}(k,z)=A(k)\exp[(k^2-l^2)^{\frac{1}{2}}z]+B(k)\exp[-(k^2-l^2)^{\frac{1}{2}}z], \tag{4}$$

and the problem reduces to finding coefficients $A(k)$ and $B(k)$ in each layer which satisfy the boundary conditions. For the two-layer model, the conditions are:

(i) the flow at the terrain surface is tangential to the surface;
(ii) at the interface between layers, $\hat{w}$ and $d\hat{w}/dz$ are continuous; and
(iii) in the upper layer, if $l_2^2>k^2$, $B_2(k)=0$ (the radiation condition), while if $l_2^2\leqslant k^2$, $A_2(k)=0$.

The usual approach is to choose an analytical expression with a simple Fourier transform to describe the terrain profile $h(x)$, the lower boundary condition, and to employ the Fourier integral to obtain analytical solutions for $w(x,z)$. Frequently, the "broad mountain assumption" is also invoked: the dominant horizontal wavelength of the flow perturbations induced by the mountain is assumed much larger than the vertical wavelength, so that $l^2\gg k^2$ and $(k^2-l^2)^{\frac{1}{2}}z\approx ilz$. We have chosen to employ a fast Fourier transform (FFT) subroutine to evaluate the Fourier integral numerically on the computer. This confers the advantage of allowing practically arbitrary terrain configurations to be used. Moreover, the broad mountain assumption is avoided. (Since neutral stability in the lower layer implies $l_1^2=0$, the accuracy of the assumption is questionable.) With the restriction to $l_2^2\geqslant l_1^2$, resonance lee waves do not occur, and no difficulties are encountered in the use of the FFT. The FFT is a finite Fourier transform, however, and imposes cyclic horizontal boundary conditions. What is modeled is thus the flow over an infinite sequence of identical mountain ridges. The domain of the flow model must be sufficiently large that the interference between successive mountains is minimal. Using a bell-shaped mountain with height 1 km and half-width 5 km, we found only very small differences in the flow patterns when the separation between peaks was reduced from 1024 to 256 km.

The discussion to this point assumes isentropic flow. Where clouds exist, $d\ln\theta/dz$ cannot be used to determine Scorer's parameter. Fraser (1970) has shown that simple substitution of θ_e for θ in (3) does not yield the correct stability criterion, and has derived the proper form of l^2 for use in saturated conditions. Inasmuch as the present work was concerned with situations involving a moist layer with a lapse rate near the moist adiabatic value, we used $l_1^2=0$ in all runs. Since this work was completed, Fraser *et al.* (1973) have described a multi-layer flow model in which conditions may change from unsaturated to saturated along a streamline. It was shown that use of Fraser's expression for l^2 in saturated air was necessary when the cloud extends to large horizontal distances from the mountain. When cloud was present only near the mountain peak, on the other hand, (3) could be used to determine the flow field with little loss of accuracy. Since some runs with our model resulted in relatively localized clouds, our use of $l_1^2=0$ may have underestimated the stability of the moist layer in these cases.

The end product of the flow model is a field of flow streamlines. Typically, 15 to 30 streamlines are provided, depending upon the depth of the moist layer and the vertical spacing between streamlines.

3. The cloud physics model

Liquid phase precipitation processes are of little significance in winter orographic storms of the type considered here. Thus the liquid water content is assumed to be entirely in the form of cloud droplets with negligible fall velocity. Water vapor and cloud water are carried in the model as the mixing ratios r_v and r_c, respctively, and are assumed to move with the air flow along streamlines.

a. Initial conditions

The vertical temperature and moisture profiles in the initial state are determined from the vertical profiles of θ_0 and θ_e; $d\ln\theta_0/dz$ and $d\ln\theta_e/dz$ are assumed constant in the moist layer. The initial moisture supply is given by the mixing ratio r_0. Along any streamline, the total mixing ratio (the sum of vapor, cloud water, and ice mixing ratios) can change only by gravitational sedimentation of ice particles.

b. Cloud formation, condensation and evaporation

The cloud water content is determined by the restriction that supersaturation with respect to the liquid

is not allowed. That is,

$$\left.\begin{aligned} &\text{if } r_c=0, \quad r_v \leqslant r_{v\,\mathrm{sat}} \\ &\text{if } r_c>0, \quad r_v=r_{v\,\mathrm{sat}} \end{aligned}\right\},$$

where $r_{v\,\mathrm{sat}}$ is the saturation vapor mixing ratio at the local temperature. Since the temperature is affected both by vertical motions and by water phase transitions through the Clausius-Clapeyron equation, there is an implicit relationship between T and $r_{v\,\mathrm{sat}}$, which is solved by a rapidly converging iteration using the Newton-Raphson method. When the cloud liquid water is exhausted and ice particles are present, $r_{v\,\mathrm{sat}}$ is set equal to the saturation mixing ratio over ice.

c. *Ice nucleation*

The number of ice nuclei, per unit volume, active at the local temperature, is computed at each space point in the model. However, ice nuclei are activated to form ice particles only when cloud water is present. Thus, as nuclei move with an ascending parcel within the cloud, more ice particles are continuously generated. However, once the parcel begins to descend and warm, no further activation of nuclei is permitted.

The number of natural nuclei per liter, active at supercooling ΔT, is taken from Fletcher (1962):

$$n_n=10^{-5}\exp(0.6\,\Delta T). \tag{5}$$

The number concentration of active artificial nuclei is calculated from

$$n_a=n_t\exp[B/(T-T_t)], \tag{6}$$

where n_t is the total concentration of nucleant particles and T_t the threshold temperatures for nucleation. On a plot of log n_a vs T, (6) gives a rectangular hyperbola with asymptotes at n_t and T_t, and the parameter B governs the sharpness of the "bend" in the curve. We have found that the measured activities of a wide variety of nucleants can be approximated by (6), by varying the parameters n_t, T_t and B. For this work, we have used three different nucleant activity curves, representing the aerosols from a typical AgI pyrotechnic device with a high mass output rate, an AgI-acetone burner with a low mass output rate, and an organic nuclei generator using the compound 1,5-dihydroxy-naphthalene (DN), developed in our laboratory. The respective activity curves are designated AgI-high, AgI-low, and DN, and are shown in Fig. 1; the parameters used in (6) to obtain these curves are given in Table 1.

TABLE 1. Parameters used in (6) for artificial ice nuclei spectra.

Nucleant	$\log_{10}n_t$	B	T_t(°C)
AgI-high output source	16.4	28	−0.8
AgI-low output source	17.5	28	−3.0
1,5-dihydroxy-naphthalene	14.7	5	−5.1

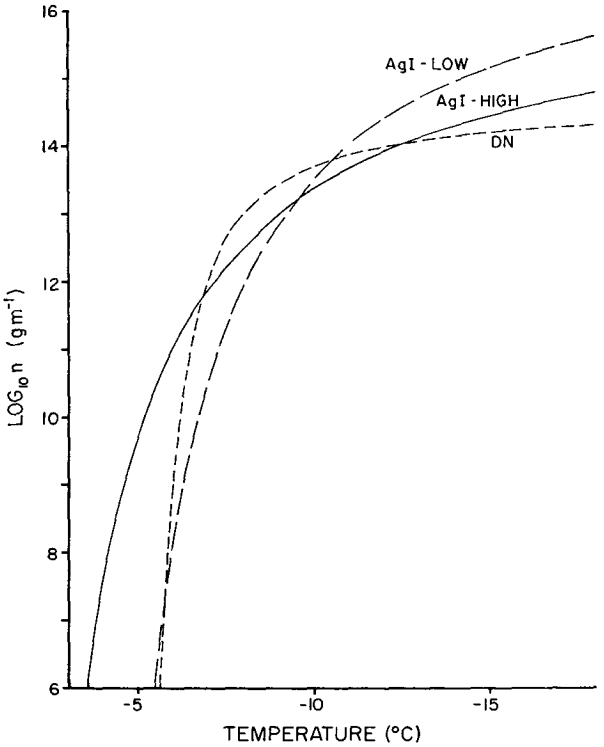

FIG. 1. Activity of artificial ice nuclei (number per gram) as a function of temperature. Solid curve: AgI-high (typical high-output AgI generator, e.g., a pyrotechnic); dashed curve: AgI-low (typical low output AgI source, e.g., an acetone burner); dotted curve: DN (the organic nucleant 1,5-dihydroxynaphthalene, as produced by supersonic nozzle expansion generator).

d. *Ice particle growth*

The model considers ice particle growth by vapor deposition and by riming. The growth of ice particles is modeled by following the evolution of a population of particles distributed in a finite number of discrete size categories. At each space point, a "bin" is provided for each size category. Activation of ice nuclei at a point results in injection of particles into the lowest bin. As the total mass of ice at a point increases, some of the particles in each bin are promoted to a higher bin in such a way as to conserve the total number of particles and the total mass of ice. The computational method is the same as that used by Kovetz and Olund (1969) for droplet growth by condensation. Seven bins are provided for ice particles growing by vapor deposition, and one bin is reserved for rimed particles. The mass per particle increases by a factor of 8 from bin to bin, for the deposition growth categories.

This particle growth scheme has two disadvantages. First, it generates considerable numerical "diffusion"

along the mass coordinate, and results in some particles reaching the larger size bins more rapidly than they should. It is equivalent to the simple "forward-upstream" finite-difference approximation to the advection equation, whose properties have been well described (Molenkamp, 1968). Since this model was constructed, Egan and Mahoney (1972) have described an unconventional difference scheme which essentially eliminates the numerical diffusion problem, at the expense of an increase in computer memory requirements and computation time. In spite of these practical drawbacks, it would be desirable to use a difference scheme such as they describe in future work. The second disadvantage of our particle growth scheme is that the use of a finite number of size categories necessitates some arbitrary decision concerning the fate of the mass added to particles in the largest size category, since no higher bin exists into which these particles can be promoted. Our choice was simply to accumulate this mass in the highest bin (bin 7 for depositional growth). The model thus inherently contains an apparent ice crystal multiplication process. Evaporation of ice crystals results in movement of particles to lower bins. When particles move down through bin 1, they are removed from the system.

Simulation of ice particle growth by vapor deposition is complicated by the dependence of ice crystal shape on temperature. The process becomes especially complicated when a particle experiences a range of temperatures along its trajectory. However, over the temperature range -8 to -25°C, the predominant growth habit at water saturation is in the form of hexagonal plates or planar dendrites (Hallett and Mason, 1958). This is also the temperature zone in which ice crystal growth is most rapid (Fukuta, 1969). We therefore assume the ice crystals to be plate-like in shape, and use Auer and Veal's (1970) data for the diameter-to-thickness ratio as a function of crystal size. The standard expression for the rate of mass growth of a spherical particle by vapor deposition (e.g., Fletcher, 1962) is used, with empirical correction factors for the non-spherical shape, ventilation factor, and growth rate variation with temperature:

$$\frac{dm}{dt}=\frac{4\pi(S-1)rF}{\left(\frac{L_s^2M}{KRT^2}\right)+\left(\frac{1}{D\rho_{sat}}\right)}, \tag{7}$$

where m is the mass of an ice sphere of radius r, S is the environmental saturation ratio with respect to ice, L_s the heat of sublimation of ice, M the molecular weight of water, R the universal gas constant, K the thermal conductivity of air, D the diffusion coefficient for water vapor in air, and ρ_{sat} the saturation vapor density with respect to ice at the environmental temperature T. The factor F contains the correction factors. Table 2 gives (in columns 1–7) the characteristics of the ice particles growing by vapor deposition, including the shape factors and ventilation coefficients. An empirical correction for the variation of growth rate with temperature is taken from Fig. 11 of Fukuta (1969). This ice growth treatment gives growth rates comparable to those predicted by Jayaweera (1971), but somewhat greater than those of Koenig (1971).

Riming growth is simulated by the simple collection equation

$$\frac{dm}{dt}=Aqv_tE, \tag{8}$$

where A is the cross-sectional area of a particle falling at terminal velocity v_t through a cloud with liquid water content q. The parameter E is the collection efficiency, which is arbitrarily set to 0.25. Rimed particles are assumed to be spheres with diameter 1.5 mm, density 0.2 g cm^{-3}, falling at 1 m s^{-1}. The properties of the rimed particles are given in column 8 of Table 2. All particles with platelet diameter >100 μm (i.e., bins 4–8) are assumed to take part in riming growth.

e. *Precipitation*

The terminal velocities of all particles are given in Table 2. If the vertical spacing between two streamlines is Δz, and the time increment is Δt, then a fraction $v_t\Delta t/\Delta z$ of the ice particles in each bin on the upper streamline is transferred to the lower streamline at each horizontal space position. The precipitation rate at the ground is given by the rate at which particles fall in this manner from the first streamline above the terrain surface.

4. The nuclei diffusion model

Nuclei are released from a point at ground level 20–45 km upwind of the mountain peak. A "point source" in a two-dimensional model, however, represents a line source normal to the plane of the model in three dimensions. Since lateral diffusion near the earth's surface is generally more rapid than vertical diffusion, the plumes from several point sources arrayed at equal intervals parallel to a mountain ridge will merge to form effectively a line source plume. In this model we assume that such sources are located 10 km apart and consider the output of a single source.

We are primarily interested in the vertical dispersion of nuclei from a source emitting continuously into an airstream with horizontal velocity U_0. In the steady state, the appropriate advection-diffusion equation (Pasquill, 1962) is then given by

$$U_0\frac{\partial n_t}{\partial x}=\frac{\partial}{\partial z}\left(K_z\frac{\partial n_t}{\partial z}\right), \tag{9}$$

where n_t is the total concentration of nuclei particles and K_z is the effective eddy diffusion coefficient. For

TABLE 2. Ice crystal characteristics

	Bin number							
	1	2	3	4	5	6	7	8
Diameter (μm)	14	32	73	170	390	890	2040	1500
Thickness (μm)	5.3	8	12	18	28	42	64	—
Terminal velocity (cm s^{-1})	0.16	0.64	2.5	10	20	35	50	100
Ventilation factor	1.01	1.03	1.08	1.26	1.55	2.15	3.05	—
Shape (capacitance) factor	1.11	1.27	1.45	1.68	1.93	2.22	2.54	—
Particle mass (gm)	2.46	1.97	1.57	1.26	1.01	8.06	6.44	3.53
$\times 10^{(\ )}$	(−10)	(−9)	(−8)	(−7)	(−6)	(−6)	(−5)	(−4)

simplicity we assume a constant diffusion coefficient of the order of 100 m^2 s^{-1}. The diffusion equation (9) is solved numerically in a rectangular coordinate system, which is then deformed along the vertical coordinate to coincide with the flow streamline field.

5. Results

The model has been used primarily with idealized initial conditions to determine the important factors governing precipitation rates and efficiencies. A few runs were made using observational data from a field program, and will be discussed briefly.

a. Idealized test cases

The number of variable parameters in the model is far too large to permit examination of a matrix of initial conditions, i.e., to determine the effects of varying each parameter in the presence of all the others. Therefore, some parameters were arbitrarily held constant in all runs. The mountain profile was the bell-shaped curve given by $h=h_0(1-x^2/b^2)^{-1}$, where x is the horizontal distance from the mountain peak, h_0 the height of the peak, and b the mountain half-width, with $h_0=1$ km and $b=5$ or 10 km. A horizontal flow velocity of 10 m s^{-1} and a moist layer 2 km deep were used in all runs. The values of θ and θ_e at the surface, and $d\ \ln\theta/dz$ and $d\ \ln\theta_e/dz$, were adjusted to give a relative humidity near 90% throughout the lower layer and a lapse rate near moist adiabatic. The variable parameters were $T_0(0)$, the surface temperature in the upstream sounding, the mountain half-width b, and the type and amount of seeding materials released 21 km upwind of the peak. The domain of the model was a region 50 km in horizontal extent with the mountain centered on the lower boundary.

Fig. 2 shows a typical flow solution with the cloudy region superimposed, for the case $T_0(0)=272.5$ K. Table 3 gives the initial temperatures and mixing ratios, $T_0(z)$ and $r_0(z)$, at the bottom and top of the moist layer, the mountain half-width b, and unseeded precipitation efficiencies for all the idealized test cases. T_0 and r_0 vary nearly linearly with height in the moist layer. The precipitation efficiency is the ratio of total

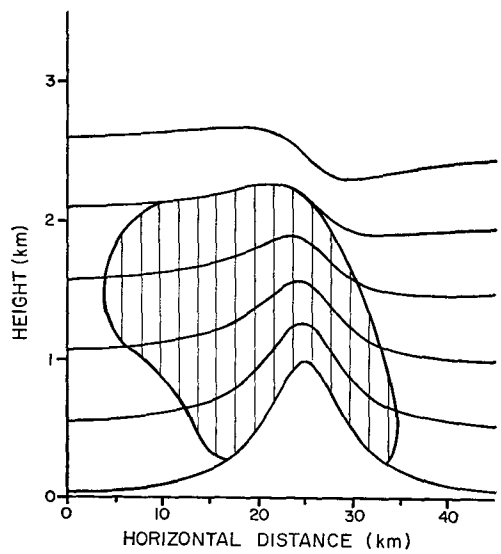

FIG. 2. Typical flow solution, for $T_0(0)=272.5$ K, showing flow streamline field with supercooled cloud (shaded region) superimposed.

TABLE 3. Initial conditions and unseeded precipitation efficiencies for idealized test cases.

Temperature $T_0(0)$ (K)	Temperature $\frac{T_0(0)}{T_0(2000)}$ (°C)	Mixing ratio $\frac{r_0(0)}{r_0(2000)}$ (g kg^{-1})	Mountain half-width b (km)	Precipitation efficiency
265	$\frac{-8.15}{-22.50}$	$\frac{2.55}{1.03}$	5	0.2805
267.5	$\frac{-5.65}{-19.95}$	$\frac{2.76}{1.15}$	5	0.2673
270	$\frac{-3.15}{-17.40}$	$\frac{3.28}{1.42}$	5	0.0274
272.5	$\frac{-0.65}{-14.85}$	$\frac{3.86}{1.74}$	5	0.0026
275	$\frac{1.85}{-12.30}$	$\frac{4.52}{2.14}$	5	0.00037
275	$\frac{1.85}{-12.30}$	$\frac{4.52}{2.14}$	10	0.0013

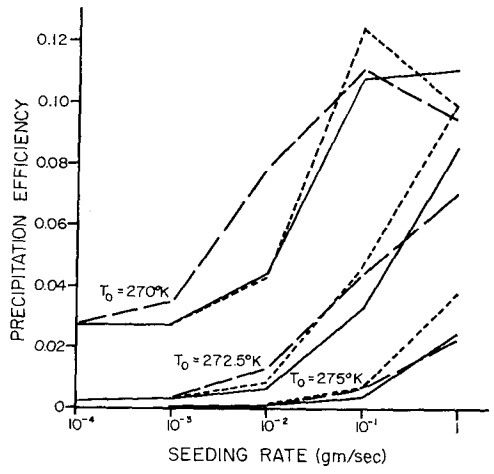

FIG. 3. Variation of precipitation efficiency with seeding rate and type of nucleant for three different initial conditions of temperature. The precipitation efficiencies are determined with respect to the precipitable water (defined in text). Solid curves: AgI-high nucleant; dashed curves: AgI-low; dotted curves: DN.

precipitation to the flux of "precipitable water," here defined as the flux of water in excess of that required for ice saturation directly above the mountain peak.

An efficient ice phase precipitation process requires a sufficient number of ice particles, an ample supply of moisture, and adequate time for ice particle growth. For natural (unseeded) clouds, the number of ice crystals formed is largely dependent upon cloud temperature, through the ice nuclei activity spectrum. The initial conditions in the model insure an ample moisture supply. The time available for growth is primarily determined by the horizontal transit time, x_c/U_0, where x_c is the horizontal dimension of the cloud along the wind vector U_0. The effect of cloud temperature in the results shown in Table 3 is strong; precipitation efficiencies increase by about an order of magnitude for $T_0(0) > 267.5$ K for each 2.5°C decrement in cloud temperature. Most of this increase is attributable to the fact that a 2.5°C change in ΔT in (5) increases n_n by about a factor of 4.5. The additional factor of 2 is largely due to the increase in ice crystal growth rate as temperature decreases. For $T_0(0) \leqslant 267.5$ K, however, the precipitation efficiency curve levels off abruptly, indicating that ample numbers of natural nuclei are now available and that further increases in ice nuclei concentrations will not produce further precipitation increases. These results are in agreement with the field results from the Climax experiment (e.g., Mielke *et al.*, 1971). The temperatures at the top of the moist layer in the initial conditions, $T_0(2000)$ in Table 3, are within 2°C of the cloud top temperatures in the model. The abrupt change in precipitation efficiency in the model thus occurs at a cloud top temperature slightly colder than −20°C. In the Climax experiment, positive seeding effects were found for cloud top temperature warmer than about −20°C, while null or negative effects were suggested for colder clouds.

The effect of ice crystal residence time alone is seen by comparison of the last two lines of Table 3, wherein the mountain half-width b was doubled while holding other conditions constant. The precipitation efficiency increased by about a factor of 4.

According to the results in Table 3, the model indicates that an efficient natural precipitation process can bring 25–30% of the precipitable water to ground level. The much lower precipitation efficiencies indicated for the cases with $T_0(0) \geqslant 270$ K suggest that precipitation augmentation by seeding would be possible. This suggestion is confirmed by the model. For each initial condition shown in Table 3, twelve seeded runs were carried out, using the three nucleant sources described in Section 3, and four seeding rates with each source. The seeding source in all cases was situated at ground level 21 km upwind of the mountain peak. A constant eddy diffusion coefficient of 100 $m^2 s^{-1}$ was used for nuclei dispersion.

The seeding rates were 10^{-3}, 10^{-2}, 10^{-1} and 1 gram of nucleant per second. Fig. 3 shows the computed precipitation efficiencies with respect to the precipitable water for all runs with $b = 5$ km, $T_0(0) \geqslant 270$ K. The most interesting features of these results are the change in the amount of nucleant required to maximize precipitation as cloud temperature increases, and the relative effects of the different nucleants.

Seeding produced marked precipitation increases for all runs with $T_0(0) \geqslant 270$ K. However, Fig. 3 shows that the seeding rate required to produce a given precipitation increase is a strong function of cloud temperature. For $T_0(0) = 270$ K, the precipitation increase reaches a maximum for seeding rates near 0.1 g s^{-1}. A seeding rate of 0.1 − 1 g s^{-1} is easily achieved using pyrotechnic devices, but acetone burner outputs are usually much lower. A typical acetone burner with an output of the order of 0.03 g s^{-1} would produce a near-optimum result for the $T_0(0) = 270$ K case (the AgI-low curve). At warmer cloud temperatures, comparable precipitation increases appear possible, but require much larger seeding rates. The reason, of course, is that both the number of active nuclei and the rate of ice crystal growth decrease as cloud temperature increases. These results suggest that use of a single fixed seeding technique for all cloud conditions is not a satisfactory approach for optimization of precipitation. Furthermore, it may not be adequate even to answer the simpler question: Under what conditions can seeding increase precipitation? For example, an AgI-acetone burner emitting 0.01 g s^{-1} produces a marked increase in precipitation for $T_0(0) = 270$ K, but only an imperceptible change for $T_0(0) = 275$ K, whereas very substantial increases are possible in the latter case at higher seeding rates. Thus a fixed seeding technique will produce significant precipitation increases in only a small part of the temperature range in which increases actually are possible.

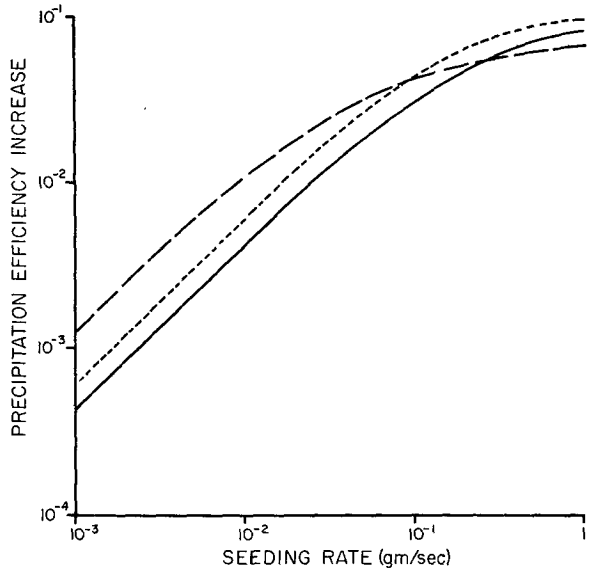

FIG. 4. Increase in precipitation efficiency (seeded minus unseeded efficiency) as a function of seeding rate for $T_0(0)=272.5$ K. Nucleant curves identified as in Fig. 3.

When $T_0(0)<270$ K, seeding produced relatively small precipitation decreases in all cases.

The relative effects of different nucleants can be understood by comparing Figs. 1 and 3. Fig. 1 shows that there is a temperature region in which each of the three nucleants surpasses the others in terms of numbers of active nuclei per gram. The AgI-high curve lies above the other two at temperatures warmer than about −7°C, DN is highest between −7 and −11°C, and the AgI-low curve is highest below −11°C. Above −7°C all the curves are two orders of magnitude or more below their values at temperatures below −10°C, so that the superiority of the AgI-high nucleant above −7°C is of little value. In practically all runs, therefore, a larger quantity of this nucleant is required to produce a given effect than for the other nucleants. The AgI-low nucleant is relatively ineffective at temperatures above −10°C; thus it is generally not an advantageous nucleant to use for warmer clouds. It is much more effective at low seeding rates for colder clouds, as is seen by comparing the relative effects of different nucleants for $T_0(0)=270$ K with those for $T_0(0)=275$ K. However, an overseeded condition is reached at cloud top more rapidly with this nucleant as seeding rates increase. The highest precipitation efficiencies for all cloud conditions were attained using DN; the abrupt rise in activity of this nucleant just above −10°C and the nearly flat spectrum at colder temperatures apparently provides sufficient ice particles for efficient precipitation formation without producing drastic overseeding at colder cloud top temperatures.

The onset of overseeding with the different nucleants is shown more clearly in Fig. 4, a log-log plot of the *increase* in precipitation efficiency (the difference between seeded and unseeded efficiencies) vs seeding rate for $T_0(0)=272.5$ K. All curves have an initial slope of unity; at low seeding rates, the increase in precipitation is directly proportional to the number of additional ice nuclei. As seeding rates increase, however, the slopes of all curves decrease. The AgI-low nucleant is most effective at low seeding rates, but its effect falls off most rapidly as seeding rate increases, due to overseeding of the cloud top.

The effect of the ice nuclei diffusion rate on seeding effects was investigated in preliminary runs with the model. Decreasing K_z from 100 to 10 m^2 s^{-1} greatly reduced the effects of seeding, but increasing K_z to 1000 m^2 s^{-1} had a relatively much smaller effect. Seeding effects are primarily determined by the number of nucleant particles reaching the cold upper regions of the cloudy layer. (The diffusion model assumes that no nuclei penetrate into the stable upper layer.) The distribution of particles in the lower, warmer regions is much less important, both because the fraction of particles which are active at these temperatures is very small, and because ice particles formed low in the cloud fall out before they attain appreciable mass. At the higher values of K_z used here, nuclei particles were very nearly uniformly distributed throughout the depth of the cloud above the mountain peak, so that further increases in seeding effect would not be expected at still greater K_z values. For $K_z=10$ m^2 s^{-1}, however, almost no nuclei reached cloud top level. For $K_z=100$ m^2 s^{-1}, the value used in the model runs reported here, the nuclei concentration at cloud top was between 20 and 50% of the limiting value for the care of a uniform vertical distribution, and the concentration at cloud top was a factor of 3–10 lower than that at terrain level. This concentration gradient appears consistent with the experimental results of Grant (1968).

b. Real data test cases

Since specification of the initial conditions for a precipitation model involves a rather large number of parameters, it was decided to run some test cases using actual field data for the initial conditions, rather than to extend the study to further idealized cases. Mr. S. R. Brown, Division of Atmospheric Water Resources Management, U. S. Bureau of Reclamation, kindly supplied a complete set of atmospheric soundings and hourly precipitation records from the Colorado River Basin Pilot Project for the winter of 1971–72. We have examined a limited number of soundings (16 in all) from snowstorms in the fall of 1971, selected to represent periods of light, moderate and heavy snowfall in the Wolf Creek Pass area of the San Juan Mountains in southwestern Colorado. To model the terrain, we used the same bell-shaped profile as in the idealized test cases, with two different values (8 and 12 km) for the mountain half-width b. The barrier height h_0 was 1350 m.

To reduce the soundings to a two-layer atmosphere, plots of θ and θ_e vs height were used to determine representative values at the top and bottom of the moist layer; then, assuming $d\ln\theta/dz$ and $d\ln\theta_e/dz$ constant, smoothed vertical profiles of temperature and mixing ratio were computed. This procedure was roughly adequate in most cases, but in two instances shallow moist layers were smoothed out to the extent that no cloud formed in the model. Since relative humidities in some of the initial conditions were near 100%, so that cloud boundaries extended far upwind of the mountain, the domain of the model was extended from 60 km upwind of the mountain peak to 15 km downwind.

Each sounding was run for $b=8$ and 12 km, with an unseeded and a seeded case for each b value. The seeding source was located 45 km upwind of the mountain peak, using the AgI-high nucleant curve at a seeding rate of 1 g s^{-1}.

The actual results of the model runs are summarized elsewhere (Fukuta *et al.*, 1973) and are not given here. The data sample is too small to permit firm conclusions to be drawn. However, there are a number of features which seemed to appear consistently in the results, although some of them must be considered as only tentatively established at this time:

1) The smoothing of the vertical moisture profiles produced by the initialization procedure for these runs has a tendency to reduce horizontal cloud dimensions for soundings in which the relative humidity varies rapidly with height. Thus the residence times of ice crystals in the cloud and the resulting precipitation were probably underestimated in these runs.

2) When the initialization procedure gave a reasonable description of cloud formation, the model generally predicted the heaviest snowfall from soundings which corresponded to heavy actual snowfall. The peak precipitation rates in these cases lie below the measured rates by a factor of 2 to 3.

3) The spatial distribution of snowfall is qualitatively in agreement with the field data, in that high wind velocities and/or warm cloud temperatures tended to give heavier precipitation on the lee side of the mountain in both model and field data.

4) Increasing the mountain half-width from 8 to 12 km increased the model precipitation, the effect being generally more pronounced for runs in which precipitation was light.

5) Deep moist layers gave substantial snowfall amounts which were not appreciably affected by seeding. The greatest relative effects of seeding were observed in runs in which the unseeded precipitation was light. It is interesting to note that in practically all cases where an appreciable positive seeding effect was found, the sounding in question was taken near the beginning or end of a storm. This result is in line with the observations of Chappell *et al.* (1971).

6. Conclusions

We have developed a two-dimensional, steady-state model of orographic ice-phase precipitation. The model has been used to investigate the dependence of natural precipitation rates on certain initial conditions, with emphasis on the effect of cloud temperature. In addition, the effects of seeding with artificial ice nuclei from ground-based nuclei sources were simulated, using different types of nucleants and variable seeding rates.

The model shows a dependence of natural precipitation efficiency on cloud top temperature which is in good agreement with field observations from the Climax experiment. Precipitation efficiencies increase steadily as cloud top temperatures decrease to about −20°C, but change little as cloud top temperatures decrease still further.

The model shows that precipitation from the warmer clouds can be enhanced by seeding with artificial ice nuclei. It also shows, however, that the quantity of seeding material required to produce a given increase in total precipitation is a strong function of cloud temperature. These results suggest that the use of a fixed seeding procedure is probably an unsatisfactory approach either for optimizing precipitation or for determining the range of conditions under which precipitation increases can be obtained by seeding.

Precipitation efficiencies were found to depend upon the activity spectrum of the seeding material as a function of temperature. In the cases studied here, the activities of the nucleants at warm temperatures were found to be of little importance, because of the relatively small total number of nuclei active in this temperature region and the small growth rate of ice crystals. Seeding results were more strongly affected by activity of the nucleants at temperatures below −7°C. The relative effectiveness of different nucleants varied with cloud temperature.

Acknowledgments. This work was supported in part by the U. S. Bureau of Reclamation under Contract 14-06-D-7048, and in part by the National Science Foundation (RANN) under Grant GI-39849. Acknowledgment is also made to the National Center for Atmospheric Research, which is sponsored by the National Science Foundation, for computer time used in this research.

REFERENCES

Auer, A. H., and D. L. Veal, 1970: The dimension of ice crystals in natural clouds. *J. Atmos. Sci.*, **27**, 919–926.

Chappell, C. F., L. O. Grant and D. W. Mielke, 1971: Cloud seeding effects on precipitation intensity and duration of winter orographic clouds. *J. Appl. Meteor.*, **10**, 1006–1010.

Egan, B. A., and J. R. Mahoney, 1972: Numerical modeling of advection and diffusion of urban area source pollutants. *J. Appl. Meteor.*, **11**, 312–322.

Fletcher, N. H., 1962: *The Physics of Rainclouds.* Cambridge University Press, 386 pp.

Fraser, A. B., 1970: Airflow through a cap cloud. *Preprints Second Conf. Weather Modification*, Santa Barbara, Calif., Amer. Meteor. Soc., 14–17.

——, R. C. Easter and P. V. Hobbs, 1973: A theoretical study of the flow of air and fallout of solid precipitation over mountainous terrain: Part I. Airflow model. *J. Atmos. Sci.*, **30**, 801–812.

Fukuta, N., 1969: Experimental studies on the growth of small ice crystals. *J. Atmos. Sci.*, **26**, 522–531.

——, M. N. Plooster, Y. Paik, L. F. Evans, A. Gorove and T.-L. Wang, 1973: The engineering, microphysical, and dynamical aspects of precipitation management. Final Report to U. S. Bureau of Reclamation, Contract 14-16-D-7048, 150 pp.

Grant, L. O., 1968: The role of ice nuclei in the formation of precipitation. *Proc. Intern. Conf. Cloud Physics*, Toronto, 305–310.

Hallett, J., and B. J. Mason, 1958: The influence of temperature and supersaturation on the habit of ice crystals grown from the vapor. *Proc. Roy. Soc. London*, **A247**, 440–453.

Hobbs, P. V., and L. F. Radke, 1973: Redistribution of snowfall across a mountain range by artificial seeding: A case study. *Science*, **181**, 1043–1045.

Jayaweera, K. O. L. F., 1971: Calculations of ice crystal growth. *J. Atmos. Sci.*, **28**, 728–736.

Koenig, L. R., 1971: Numerical modeling of ice deposition. *J. Atmos. Sci.*, **28**, 226–237.

Kovetz, A., and B. Olund, 1969: The effect of coalescence and condensation on rain formation in a cloud of finite vertical extent. *J. Atmos. Sci.*, **26**, 1060–1065.

Mielke, P. W., L. O. Grant and C. F. Chappell, 1971: An independent replication of the Climax wintertime orographic cloud seeding experiment. *J. Appl. Meteor.*, **10**, 1198–1212.

Molenkamp, C. R., 1968: Accuracy of finite-difference methods applied to the advection equation. *J. Appl. Meteor.*, **7**, 160–167.

Pasquill, F., 1962: *Atmospheric Diffusion.* Princeton, N. J., Van Nostrand, 297 pp.